Laboratory demonstration of a broadband six-level phase mask coronagraph

Fabien Patru, Pierre Baudoz, Raphaël Galicher, Qing Cao, Kai Wang, Lujing Xing, Faouzi Boussaha, Josiane Firminy, Marion Bonafous

Research Article | Vol. 26, No. 8 | 16 Apr 2018 | OPTICS EXPRESS 10007
Optics EXPRESS

Laboratory demonstration of a broadband six-level phase mask coronagraph

FABIEN PATRU,[1,*] PIERRE BAUDOZ,[1] RAPHAËL GALICHER,[1] QING CAO,[2] KAI WANG,[2] LUJING XING,[2] FAOUZI BOUSSAHA,[3] JOSIANE FIRMINY,[3] AND MARION BONAFOUS[1]

[1]*PSL Research Univ., CNRS, Sorbonne Univ., UPMC Univ. Paris 06, Univ. Paris Diderot, Sorbonne Paris Cité, Observatoire de Paris, LESIA, 5 place Jules Janssen, 92195 Meudon cedex, France*
[2]*Department of Physics, Shanghai Univ., 99 Shangda Road, Baoshan District, Shanghai 200444, China*
[3]*PSL Research Univ., CNRS, Sorbonne Univ., UPMC Univ. Paris 06, Univ. Paris Diderot, Sorbonne Paris Cité, Observatoire de Paris, GEPI, 5 place Jules Janssen, 92195 Meudon cedex, France*
[*] *fabien.patru@gmail.com*

Abstract: The six-level phase mask (SLPM) can be used in a focal plane as an efficient coronagraph [Opt. Express **22**, 1884 (2014)]. It has several advantages: high-contrast imaging in broadband with small inner working angle; easy fabrication at low cost by photolithography and reactive ion etching processes; easy implementation with no need of pupil apodization. We present in this paper the first laboratory results demonstrating the high performance of a SLPM with an unobscured pupil. The on-axis attenuation reaches 2×10^{-5} at $\lambda = 800$ nm and is better than 10^{-4} over a 10% spectral bandwidth and better than 10^{-3} over a 20% bandwidth. Finally, the detection of a planet can be achieved down to 1 λ/D.

OCIS codes: (120.4820) Optical systems; (050.5080) Phase shift; (220.4840) Testing.

References and links

1. F. Hou, Q. Cao, M. Zhu and O. Ma, "Wide-band six-region phase mask coronagraph," Opt. Express **22**, 1884–1895 (2014).
2. Y. Ge, Q. Cao, R. Hu, K. Wang and X. Tong, "Cascade six-level phase-mask achromatic coronagraph," Appl. Opt. **55**, 1006–1011 (2016).
3. D. Mawet, E. Serabyn, D. Moody, B. Kern, A. Niessner, A. Kuhnert, D. Shemo, R. Chipman, S. McClain and J. Trauger, "Recent results of the second generation of vector vortex coronagraphs on the high-contrast imaging testbed at JPL," Proc. of the SPIE **8151**, 815108 (2011).
4. D. Rouan, P. Riaud, A. Boccaletti, Y. Clénet and A. Labeyrie, "The four-quadrant phase mask coronagraph. I. Principle," Publications of the Astron. Soc. of the Pacific **112**, 1479–1486 (2000).
5. P. Riaud, A. Boccaletti, D. Rouan, F. Lemarquis and A. Labeyrie, "The four-quadrant phase mask coronagraph. II. Simulations," Publications of the Astron. Soc. of the Pacific **113**, 1145–1154 (2001).
6. P. Riaud, A. Boccaletti, J. Baudrand and D. Rouan, "The four-quadrant phase mask coronagraph. III. Laboratory performance," Publications of the Astron. Soc. of the Pacific **115**, 712–719 (2003).
7. A. Boccaletti, P. Riaud, P. Baudoz, J. Baudrand, D. Rouan, D. Gratadour, F. Lacombe and A. M. Lagrange, "The four-quadrant phase mask coronagraph. IV. First light at the very large telescope," Publications of the Astron. Soc. of the Pacific **116**, 1061–1071 (2004).
8. P. Baudoz, A. Boccaletti, P. Riaud, C. Cavarroc, J. Baudrand, J. M. Reess and D Rouan, "Feasibility of the four-quadrant phase mask in the mid-infrared on the James Webb space telescope," Publications of the Astron. Soc. of the Pacific **118**, 765–773 (2006).
9. M. Bonafous, R. Galicher, P. Baudoz, J. Firminy and F. Boussaha, "Development and characterization of four-quadrant phase Mask coronagraph (FQPM)," Proc. of the SPIE **9912**, 99126J (2016).
10. P. Baudoz, R. Galicher, F. Patru, O. Dupuis and S. Thijs, "Status and performance of the THD2 bench in multi-deformable mirror configuration," Adaptive Optics for Extremely Large Telescopes conf. **5**, 1–9 (2017).
11. J. Mazoyer, P. Baudoz, R. Galicher and G. Rousset, "High-contrast imaging in polychromatic light with the self-coherent camera," Astron. and Astrophys. **564**, L1 (2014).
12. J. R. Delorme, M. N'Diaye, R. Galicher, K. Dohlen, P. Baudoz, A. Caillat, G. Rousset, R. Soummer and O. Dupuis, "Laboratory validation of the dual-zone phase mask coronagraph in broadband light at the high-contrast imaging THD testbed," Astron. and Astrophys. **592**, A119 (2016).

#315110 https://doi.org/10.1364/OE.26.010007
Journal © 2018 Received 6 Dec 2017; revised 19 Jan 2018; accepted 5 Feb 2018; published 6 Apr 2018

Optics EXPRESS

1. Introduction

Since two decades, more than 3,500 exoplanets have been discovered by using different techniques. While radial velocity and transit techniques are efficient to probe exoplanets with short orbits, the study of long-orbit planets requires direct imaging and coronagraphic techniques. However, the coronagraph must deal with planets that are 10^4 to 10^{10} fainter than their hosting star at a fraction of arcsecond, requiring efficient coronagraphs at short angular separations.

Phase masks proved to be a good solution in monochromatic or limited spectral bandwidth but expansion to broadband requires complex phase achromatization. We propose for that to use a new six-level phase mask (SLPM) coronagraph [1, 2]. Other solutions use photonic crystals, subwavelength grating or liquid crystal polymers [3] but they need a large number of manufacturing steps which can rapidly increase the fabrication defects of the component. A simpler solution is to use a well controlled fabrication process like photolithography and reactive ion etching and to optimize the azimuthal phase distribution like achieved in the SLPM.

The SLPM is a sibling of the Four-Quadrant Phase Mask (FQPM) [4–8], both using a focal plane mask that creates phase shifts in sectors of the image for producing destructive interferences in the following pupil plane. Using six sectors instead of four quadrants enables to mitigate the chromatic effects of the FQPM made of one single piece of material with two thicknesses.

The objective of this paper is to report the manufacturing process and the laboratory demonstration of a phase mask that was theoretically proposed by University of Shanghai [1, 2]. We show here: (i) the feasibility of a SLPM at Paris Observatory for any wavelength, based on our previous experience to fabricate similar FQPM components [9]; (ii) the coronagraphic efficiency of the SLPM in laboratory with respect to the wavelength.

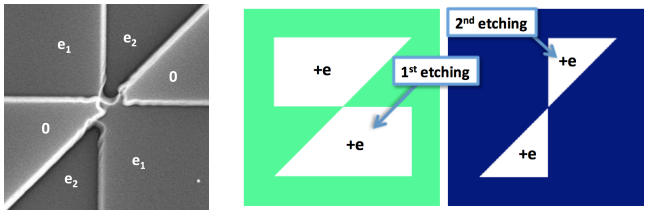

Fig. 1. Left: Image of the SLPM obtained with a scanning electron microscope. The non-uniform illumination is due to the accumulation of electrons on the transitions. Right: Lithography masks used for etching the SLPM in two steps.

2. Design and manufacturing

The SLPM is a thin silica glass split in six sectors yielding to uniform phase shifts of 0, π or 2π at the specified wavelength λ_0. The phase shifts are directly related to the etching depths by: $\phi_i = 2\pi(n(\lambda) - 1)\, e_i/\lambda$ with $n(\lambda)$ the optical index of the SiO_2 material. We can choose the optimal wavelength λ_0 for which the coronagraph totally attenuates the on-axis source (in theory). The resulting phase mask that we manufactured has been designed for an optimal wavelength $\lambda_0 = 785$ nm which requires depths of the etching equal to $e_1 = 865$ nm and $e_2 = 2 \times e_1 = 1730$ nm. If the mask is perfect, the attenuation of an on-axis point source is infinite at λ_0 and remains strong over a spectral bandwidth of 10-20% [1] (Sect. 3.2) with an inner working angle close to 1 λ/D (Sect. 3.3).

The main drawback of the SLPM is that the zones along the horizontal and vertical transitions are hardly usable for exoplanet detection, like for the FQPM [4]. Those transitions induce a close to π phase shift that attenuates and distorts the exoplanet image. At the optimal wavelength λ_0, the diagonal transition corresponds to a 0-2π variation that should not change the planet image. However, at $\lambda \neq \lambda_0$, the phase shift departs from 0-2π and the planet flux is slightly attenuated. A calibration of the transmission along the diagonal transition is thus required (Sect. 3.4).

Optics EXPRESS

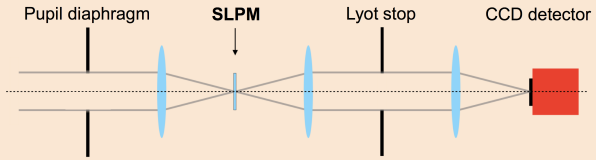

Fig. 2. Optical scheme of the laboratory experiment showing the main optical components. Left to right: Pupil diaphragm, SLPM focal phase mask, Lyot stop, CCD detector.

The SLPM is manufactured in the same way as a FQPM [9] by using the standard 365nm UV photolithography providing components at a reasonable price. The six-sectors patterns are first defined by photolithography on a 1.5-mm thick silica substrate by using two lithography masks (Fig. 1). The depth of e_1 and e_2 are then defined by lapping the uncoated sectors by reactive ion etching process in two steps. The main requirement is to ensure the same depth e for the two successive etchings so that $e_1 = e$ and $e_2 = 2e$. The sector depths e_1 and e_2 are checked by using contact profilometry technique providing an accuracy of 10 nm (depending in practice to the surface quality achieved for etching the SLPM). It gives $e_1 = 865\pm 10$ nm and $e_2 = 1710\pm 10$ nm. The other requirement is the alignment of the second etching with the first etching which is essential for maintaining the high-level performance. The visual aspect of the SLPM transitions is inspected with a scanning electron microscope (Fig. 1). Here the centering of the two masks is accurate since all the transitions are well-aligned and have almost the same narrow width. Other defects (*e.g.* transition width) can be neglected in a first order approximation.

3. Results

3.1. Experimental protocol

The SLPM has been tested at LESIA onto the facility named THD2 (*Très Haute Dynamique* in French, meaning *high-dynamic range*). The THD2 bench [10] was built to study and compare high-contrast imaging techniques in the context of exoplanet science. It allows reducing the starlight below a 10^{-8} contrast level in visible/near-infrared [11, 12].

The SLPM focal mask acts as coronagraph in the focal plane downstream of the entrance pupil (with no need of apodization) and upstream of the Lyot stop (Fig. 2). The Lyot diaphragm has a diameter of 6.5 mm which corresponds to an 80% filtering of the diameter of 8.1 mm of the unobscured entrance pupil. The images of interest are recorded on a detector located in the final focal plane optically conjugated to the phase mask focal plane. We used three laser diodes (638 nm, 705 nm and 785 nm) or 10-nm narrow-band filters in the visible plus a super continuum source. The resolution element λ/D varies from 7 to 11 pixels between 550 and 950 nm.

For the photometric calibration, we record on the detector a point spread function (PSF) for each spectral channel, keeping the Lyot stop in position. The PSF is shifted at a position far from the transitions so that the beam pass through the phase mask and the Lyot stop without being strongly attenuated. Then, we record the images of interest: centered on the SLPM (Sect. 3.2) or out of the center of the SLPM (Sect. 3.3 and 3.4). An *X-fiber* is used to extract 1% of the flux injected on the THD2 bench, while another 50%-50% X-fiber feeds a fluxmeter and a spectrometer [10]. Finally, we record simultaneously one coronagraphic image, one spectrum and one integrated flux enabling to calibrate the fluxes and the wavelengths.

We estimate the maximum of each PSF (I_{PSF}) and each off-axis image (I_{Off}) using a 2D Gaussian fit. We call τ_{Off} the transmission of an off-axis source which is equal to:

$$\tau_{Off} = \frac{Max(I_{Off})}{Max(I_{PSF})} \times \frac{F_{PSF}}{F_{Off}} \tag{1}$$

with F_{PSF} and F_{Off} the injected flux measured on the fluxmeter.

Optics EXPRESS

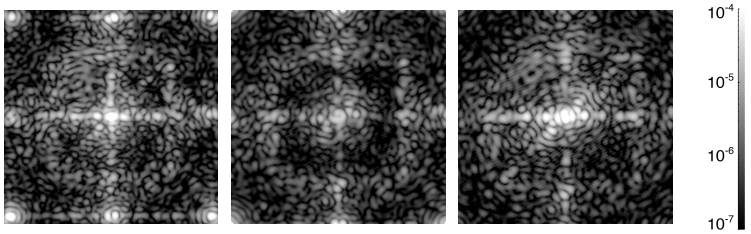

Fig. 3. On-axis coronagraphic images obtained on the THD2 bench at 730 nm (left), 800 nm (middle) and 870 nm (right). The dark hole has a width of about $27 \times 27\ \lambda/D$.

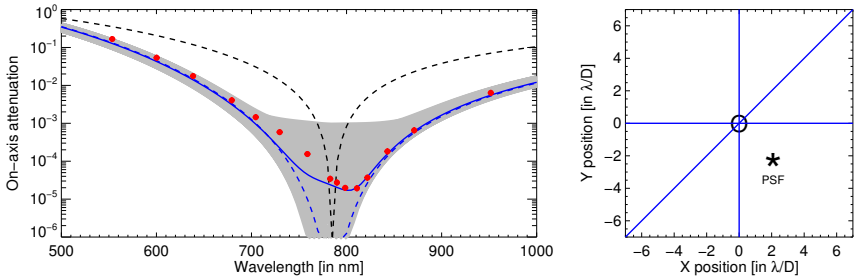

Fig. 4. Left: On-axis attenuation as a function of the wavelength. Theoretical performance of the FQPM (dark dashed curve) and the SLPM (blue dashed curve) optimized at 785 nm. Experimental data (red points) of the SLPM. Simulated data (gray zone) for e_1 varying over the range 855 – 866 nm and for e_2 varying over 1700 – 1740 nm. Simulated data (blue curve) for $e_1 = 866$ nm and $e_2 = 1726$ nm. Right: Positions in the focal plane where the on-axis attenuation (circle) and the PSF (asterisk) is measured.

For the centered coronagraphic images (I_{Coro}), we measure the maximum over the four central pixels $Max(I_{Coro}(0))$. We denote τ_{On} the on-axis attenuation:

$$\tau_{On} = \frac{Max(I_{Coro}(0))}{Max(I_{PSF})} \times \frac{F_{PSF}}{F_{Coro}} \tag{2}$$

with F_{Coro} the flux measured on the fluxmeter.

3.2. On-axis attenuation

The on-axis attenuation is estimated from experimental data for each spectral filter between 550-950 nm (Fig. 3 and Fig. 4). While the SLPM prototype have been designed at 785 nm, it performs the maximum on-axis attenuation at 800 nm by reaching 2×10^{-5}. The SLPM preserves an attenuation better than 10^{-4} between 760 nm and 830 nm (10% bandwidth) and better than 10^{-3} between 720 nm and 880 nm (20% bandwidth).

We used a numerical model to simulate a plate of glass with two varying steps (e_1 and e_2) and no defect. The focal pattern falling onto the focal mask is multiplied by a phase map on infinite size split in sectors (yielding a 0, π or 2π phase shift at the optimal wavelength). The transitions between each sector are perfectly thin. The theoretical performance of the FQPM and the SLPM (Fig. 4) assumes perfect coronagraphs with perfect thicknesses of the etching (such as $e_2 = 2 \times e_1$). Simulations show that any departure of the sector depths reduces the on-axis attenuation and can change the optimal wavelength of the phase mask. We explore values of the depths varying over the range $e_1 = 860 \pm 6$ nm and $e_2 = 1720 \pm 20$ nm (Fig. 4, gray zone). The best least squares fit gives $e_1 = 866$ nm and $e_2 = 1726$ nm (Fig. 4, blue curve). The value of e_1 is consistent with the measurements on the contact profilometer (Sect. 3.1). However, the value of e_2 is two times the standard deviation (±10%) of those profilometric measurements.

Optics EXPRESS

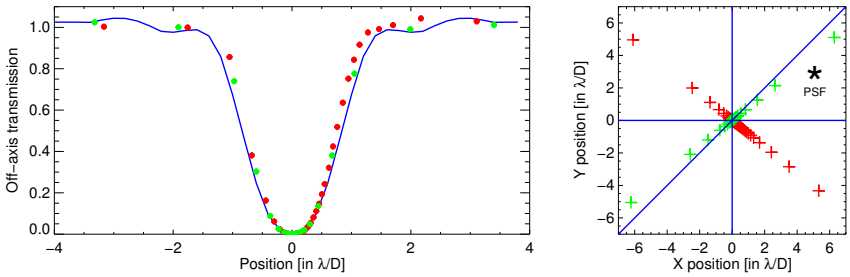

Fig. 5. Left: Off-axis transmission at 785 nm as a function of the distance from the optical axis either perpendicular (red) or parallel (green) to the diagonal transition. Simulated data (blue curve) for e_1 = 866 nm, e_2 having no effect here. The inner working angle is close to 1 λ/D. Right: Positions of the measurements in the focal plane.

3.3. Off-axis transmission

We study the off-axis transmission of the component at 785 nm by recording non-coronagraphic PSF when the star beam is not centered on the phase mask. The transmission increases as a function of the off-axis distance (Fig. 5). The inner working angle is close to 1 λ/D for which the attenuation equals to 50%. Moving in parallel or perpendicular to the diagonal transition yields to rather the same curves since this transition does not affect the transmission at 785 nm.

Undersizing the Lyot diameter compared to the pupil diameter (by 80% here) yields to a total throughput of 64%. However, the throughput is higher than 100% in Fig. 5 for some off-axis distances due to the normalization using the source far from the optical axis. The phase mask induces light interferences in the Lyot stop plane and can bring additional light from the edge of the pupil inside the Lyot stop.

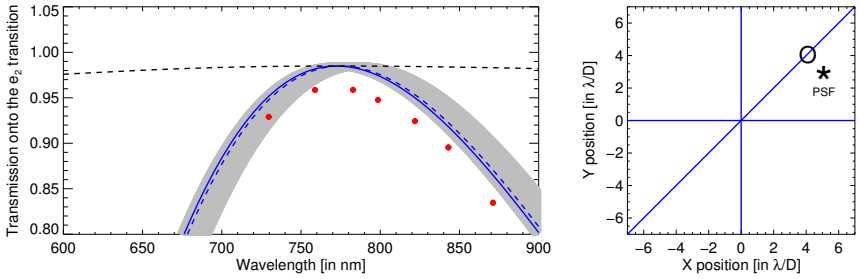

Fig. 6. Left: Transmission onto the diagonal transition as a function of the wavelength. Theoretical performance of the FQPM (dark dashed curve) and the SLPM (blue dashed curve) optimized at 785 nm. Experimental data (red points) of the SLPM. Simulated data (gray zone) for e_1 varying over the range 855 – 866 nm and for e_2 varying over 1700 – 1740 nm. Simulated data (blue curve) for e_2 = 1704 nm, e_1 having no effect here. Right: Positions of the measurements in the focal plane.

3.4. Transmission onto the diagonal transition

We study the chromaticity of the diagonal transition at a radial distance of $\approx$ 5.7 λ/D in the spectral range 730-870 nm (Fig. 6). The maximum transmission occurs at 772.5 nm, meaning that the depth e_2 is 1704 nm at 5.7 λ/D. The transmission on the diagonal transition decreases by less than 3% between 730 nm and 820 nm (10% bandwidth) and by less than 10% between 700 nm and 860 nm (20% bandwidth). The numerical model is used to explore values of the

Optics EXPRESS

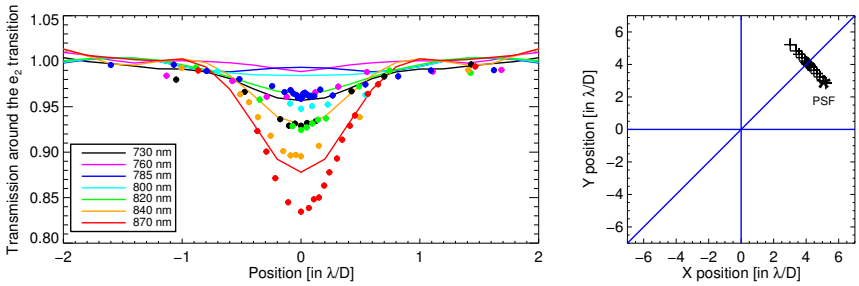

Fig. 7. Left: Transmission as a function of the wavelength when moving the source through the diagonal transition. Experimental data (big points). Simulated data (solid lines) for $e_2 = 1704$ nm. Right: Positions of the measurements in the focal plane.

depth varying over the range 1720 ± 20 nm (Fig. 6, gray zone). The best least squares fit gives $e_2 = 1704$ nm (Fig. 6, blue curve). The thickness e_1 has no effect at that location.

We also consider the chromatic behavior around the diagonal transition. The off-axis PSF is moved perpendicularly to this transition at various distances and for various wavelengths (Fig. 7). The throughput is slightly reduced up to a distance of $\pm$ 0.7 λ/D from the transition, meaning that the zone of absorption induced by the diagonal transition has a width of about 1.4 λ/D whatever the wavelength. As expected, the chromatic effects are not negligible and a photometric calibration along the diagonal transition will be required if the mask is used for astrophysical observations. Note that the experimental measurements are lower in transmission than the numerical simulations by up to 4%. The simple numerical model does not account for the transition widths which are not infinitely thin (see Fig. 1). The diagonal transition thus diffracts part of the light, yielding to an additional flux loss of few percents.

4. Conclusion

Following a theoretical work [1], we easily manufactured a six-level phase mask (SLPM) for broadband coronagraphy at very low cost. The first component show very good coronagraphic performance in laboratory, that is an on-axis attenuation of 2×10^{-5} at $\lambda = 800$ nm with a spectral filter of $\approx 1\%$ bandwidth. The attenuation remains better than 10^{-4} over a 10% bandwidth and better than 10^{-3} over a 20% bandwidth. The diagonal transition attenuates an off-axis source by less than 3% over a 10% bandwidth and by less than 10% over a 20% bandwidth.

The design was chosen with $e_1 = 865$ nm and $e_2 = 1730$ nm providing a theoretical optimized wavelength $\lambda_0 = 785$ nm whereas the best experimental on-axis attenuation occurs at 800 nm (Fig. 4, Sect. 3.2). We used a simple numerical model which does not exactly fit all the measurements but enables to understand this chromatic effect. The purpose here is not to fully model all the effects, but to show that despite of small manufacturing defects, the simulations are rather close to the experimental results. The simulation only accounts for both etching thickness errors which are by far the most critical parameters (Sect. 2), as pointed out for the 4QPM made by a single etching step. The best least squares fits of the experimental data correspond to $e_1 = 866$ nm and $e_2 = 1726$ nm for the on-axis attenuation (Fig. 4, Sect. 3.2) and to $e_2 = 1704$ nm for the transmission onto the diagonal (Fig. 6, Sect. 3.4). Optimizing the etching process will certainly improve the performance of future components.

Finally, the advantages of the SLPM coronagraph are: (i) a high contrast at small inner working angle down to 1 λ/D in broadband; (ii) an easy-to-manufacture phase mask at low cost; (iii) an easy-to-implement device with a unique focal plane mask (no need of pupil apodization). The cons are: (i) the need for calibration of the mask transmission over the field of view near the diagonal transition; (ii) the unusable field of view along the horizontal and vertical transitions.